

On the Phase Structure of the 3D Edwards Anderson Spin Glass

Enzo Marinari^(a), Giorgio Parisi^(b) and Juan J. Ruiz-Lorenzo^(b)

^(a) Dipartimento di Fisica and INFN, Università di Cagliari

Via Ospedale 72, 07100 Cagliari (Italy)

`marinari@ca.infn.it`

^(b) Dipartimento di Fisica and INFN, Università di Roma *La Sapienza*

P. A. Moro 2, 00185 Roma (Italy)

`giorgio.parisi@roma1.infn.it` `ruiz@chimera.roma1.infn.it`

February 17, 1998

Abstract

We characterize numerically the properties of the phase transition of the three dimensional Ising spin glass with Gaussian couplings and of the low temperature phase. We compute critical exponents on large lattices. We study in detail the overlap probability distribution and the equilibrium overlap-overlap correlation functions. We find a clear agreement with off-equilibrium results from previous work. These results strongly support the existence of a continuous spontaneous replica symmetry breaking in three dimensional spin glasses.

1 Introduction

Recent numerical simulations [1, 2] have given a strong numerical evidence of the existence of a spin glass phase transition in the 3D Edwards Anderson spin glass (for a critical point of view see [3]). The first studies of such models are today 15 years old (for a recent review see [4]), and the Replica Symmetry Breaking (RSB) mean field solution [5] is found to describe the most of the properties observed in finite dimensional models. The first issue is the study of the probability distribution of the order parameter $P(q)$, but the innovative features of the RSB solution inspire many questions that can be answered numerically.

Recently many of these issues have indeed been analyzed numerically. Correlation functions and block overlaps of the 3D spin glass have been shown in [6] to have a mean field like behavior, the 4D model has been studied in detail in [7], and the role of the upper critical dimension, $D_c^U = 6$, has been analyzed in [8]. It is also remarkable that a deep relation among static and dynamic behavior has been shown to be valid, for the 3D and 4D models, in [9]. At last it is worth to remind the reader that results about the transition in field in finite dimensional models have been obtained in [10, 11].

Here we try to push these results to the limit allowed by the computers we can use today, and by the numerical improved algorithms we use for our simulations. We consider the 3D spin glass with gaussian couplings, that make safer the approach to the low T region (because of the absence of accidental degeneracy) and allow to check for universality when comparing to the results of [1, 2]. After defining our model and our statistical quantities and giving details about the numerical simulations we determine critical exponents by analyzing the overlap Binder cumulant and the spin glass susceptibility in section (4). We analyze in detail the behavior of $P(q)$ in (5), by checking in detail the presence of a mean field like behavior. We analyze the behavior of a simple function in (6). In section (7) we are able to compute equilibrium correlation function, for all states and for the zero overlap sector of the theory, and to show that these results coincide with the one obtained by using an extrapolation in [6].

2 The Model

We consider a three dimensional (3D) Edwards Anderson spin glass model with Gaussian quenched random couplings J . The model is defined on a simple cubic lattice with periodic boundary conditions. The Hamiltonian of the system is

$$\mathcal{H} \equiv - \sum_{\langle ij \rangle} \sigma_i J_{ij} \sigma_j , \quad (1)$$

where by $\langle ij \rangle$ we indicate that the sum runs over couples of first neighboring sites. The J_{ij} are quenched Gaussian variables with zero mean and unit variance. We consider two real replicas of the system (in the same realization of the disorder). We define the overlap among the two real replicas α and γ at site i as

$$q_{J,i}^{\alpha,\gamma} \equiv \sigma_i^\alpha \sigma_i^\gamma , \quad (2)$$

(where the subscript J reminds us that we are in a fixed realization of the quenched disorder J), and a total overlap

$$q_J^{\alpha,\gamma} \equiv \frac{1}{V} \sum_i q_i^{\alpha,\gamma} , \quad (3)$$

where we will frequently ignore the superscripts, and denote it by q . Its probability distribution for a given sample (defining $\langle \dots \rangle$ the thermodynamical average) is

$$P_J(q) \equiv \langle \delta(q - q_J^{\alpha,\gamma}) \rangle , \quad (4)$$

and averaging over samples (denoting with $\overline{\dots}$ the average on the disorder) we define

$$P(q) \equiv \overline{P_J(q)} . \quad (5)$$

The overlap Binder parameter is defined as

$$g \equiv \frac{1}{2} \left[3 - \frac{\overline{\langle q^4 \rangle}}{\overline{\langle q^2 \rangle}^2} \right] . \quad (6)$$

The spatial overlap-overlap correlation function is

$$C_{i,j} \equiv \overline{\langle q_i q_{i+j} \rangle} = \overline{\langle \sigma_i \tau_i \sigma_{i+j} \tau_{i+j} \rangle} = \overline{\langle \sigma_i \sigma_{i+j} \rangle^2} . \quad (7)$$

We will denote by C_j (or $C(j)$) the $q - q$ correlation at distance j , averaged over different site couples whose distance is j .

It is also possible and interesting to define a correlation function where the overlap is fixed to a given value: one selects couples of equilibrium configurations (the two real replicas that constitute our system) with a given fixed overlap q and compute the correlation function among these configurations. We will denote these correlation functions with the symbol $C_q(x)$. Obviously

$$C(x) = \int dq P(q) C_q(x) , \quad (8)$$

i.e. $C(x)$ is the sum of $C_q(x)$ weighted with the static probability distribution of the overlaps. Finally we will define the connected correlation functions, by using the symbols $\hat{C}_q(x)$ and \hat{C} ,

$$\begin{aligned} \hat{C}_q(x) &= C_q(x) - q^2 , \\ \hat{C}(x) &= C(x) - \overline{\langle q^2 \rangle} . \end{aligned} \quad (9)$$

Some crucial properties of the propagators, as computed in the RSB framework, will be useful in the following (see [12] and references therein). At tree level one finds that (in dimension $D < D_c^u = 6$ there are corrections, and the contributions due to the anomalous dimension has to be included)

$$\hat{C}_q(x) \propto \begin{cases} x^{4-D} & \text{if } q = 0 , \\ x^{3-D} & \text{if } 0 < q < q_{\text{EA}} , \\ x^{2-D} & \text{if } q = q_{\text{EA}} . \end{cases} \quad (10)$$

We have based the analysis of the numerical results of our numerical simulations on finite size scaling techniques. When changing the temperature T and the lattice size L the overlap susceptibility $\chi \equiv V\overline{\langle q^2 \rangle}$ scales, in all generality, as

$$\chi(L, T) = L^{\frac{2}{\nu}} \left(h_1 \left(L^{1/\nu}(T - T_c) \right) + L^{-\omega} h_2 \left(L^{1/\nu}(T - T_c) \right) + O(L^{-2\omega}) \right) , \quad (11)$$

and the overlap Binder parameter scales as

$$g(L, T) = f_1 \left(L^{1/\nu}(T - T_c) \right) + L^{-\omega} f_2 \left(L^{1/\nu}(T - T_c) \right) + O(L^{-2\omega}) , \quad (12)$$

where ω is the exponent that determines the corrections to the scaling (it is the derivative of the β -function at the critical coupling, [14]), and f_1, f_2, h_1 and h_2 are universal functions. In particular this effect is important for the overlap Binder parameter at $T = T_c$, and gives scaling violations at the infinite volume critical point. One has that

$$g(L, T_c) = f_1(0) + L^{-\omega} f_2(0) + O(L^{-2\omega}) . \quad (13)$$

This effect explains why there is not an unique crossing point of the Binder cumulant curves (see, for instance, reference [15]), and has to be considered in the analysis of the numerical data. A one loop field theoretical computation [13] gives

$$\omega = 6 - D , \quad (14)$$

i.e. in $D = 3$ at first order in perturbation theory one expects $\omega = 3$. Of course this number will be modified by renormalization, but we expect the correct result not to be far from the previous guess. In a related theory, the four dimensional site percolation, also described by a generalized ϕ^3 theory, an exponent for the corrections to scaling $\omega \simeq 1.13$ has been determined numerically. That has to be compared to the naive (one loop) expectation, $\omega = 2$, and to the three loop value (with Padé resummation), $\omega = 1.52$ [16]. In spin glasses the computer power available at present does not allow an accurate estimate of the correction to scaling exponent.

3 Numerical Methods

We will base our discussion on large scale simulations of three dimensional systems of linear size $L = 4, 6, 8, 10, 12$ and 16 . The (earlier) simulations on smaller lattices use the tempering updating scheme [17], while (more recent) simulations on larger lattices use the parallel tempering updating scheme [18], which turns out to be very effective (see [19] for a review of improved methods, and [2] for recent work relevant for spin glasses). In all cases checking that the systems were, as far as we could establish, fully thermalized, has been the first of our worries.

We have used the APE-100 parallel supercomputer [20]. Some of the first runs have used the *tube* version (with 128 processors), while the bulk of the simulations have been run on the *tower* version, with 512 processors, with a peak performance of 25 Gflops. On the *tower* our codes has a sustained speed of 6 Gflops, and updates 200 million spins per second (even if spins can only take two values, the model is based on Gaussian couplings, and floating point arithmetics is needed).

The simulated tempering method [17, 18] (together with multicanonical approaches, see [2] and references therein) is a quantum leap for simulations of systems with a complex phase space. One can now thermalize, in the broken phase, systems that could never be studied with normal Monte Carlo. Normal tempering works quite easily up to $L = 10$ at $T \simeq 0.70T_c$ (even if the fine tuning of the g constants of [17] is somehow cumbersome). For larger lattices, $L = 12$ and 16 , we have found the use of parallel tempering [18] mandatory. As a negative *caveat* we feel like adding that using 2 months of CPU of our 25 Gflops computer we have not been able to thermalize a $L = 24$ lattice in the low temperature phase (down to $0.7T_c$).

The common characteristic of tempering and parallel tempering is that the temperature becomes a dynamical variable. In the simulated tempering we propose to update the temperature of the system at run time, after one or more usual Monte Carlo sweeps of all the spins. This fact makes possible to go from the paramagnetic phase to the spin glass phase and back; these changes enable the system to avoid the high free energy barriers that separate pure states, making possible to escape from the dynamical traps (the metastable states).

The parallel tempering is far easier to program than the simulated tempering. While in the simulated tempering we need to estimate with good precision, in a series of thermalization runs, the relative free energy of two systems at two contiguous temperatures (in the set of the allowed T values), in the parallel tempering method this problem is solved by the dynamics itself (i.e. the method generates, at run time, the correct free energies). For more details see references [17, 18, 4, 19]. For sake of completeness we give here the scheduling of the two approaches. In the simulated tempering method the process is:

1. We perform N_{TERM} iterations at a fixed temperature T_A using the Metropolis algorithm.
2. We perform N_{FE} steps with the Metropolis algorithm at the same temperature T_A that will be used to compute a first guess for the relative free energies.
3. We repeat the steps 1 and 2 following an annealing procedure (i.e. we start with the highest temperature and finish with the coldest using the final configuration of a given temperature as the initial configuration for the next lower temperature).
4. We perform five cycles of Metropolis plus simulated tempering runs (five series of one Metropolis sweep of all the lattice spins at fixed T plus one trial T update), at the end of each we tune the values of the relative free energy to make the system visiting each allowed T value for the same time. The total number of steps (for the five cycles) is N_{UFE}
5. Finally we perform N_{MEASURES} steps, measuring the interesting physical quantities.

We report in table (1) the values of the parameters used in the simulated tempering runs.

As we already said parallel tempering is simpler. Here there are no free parameters to be fine tuned. We first run N_{TERM} thermalization sweeps of the N_β copies of the system (each at a different T value), using from the start a Monte Carlo sweep for the spins followed by trial temperature sweeps among the copies. After thermalizing we run

L	Samples	N_{TERM}	N_{FE}	N_{UFE}	N_{MEASURES}
4	33200	10000	10000	50000	10000
4	2048	200000	350000	2000000	10^6
6	2048	200000	500000	2.5×10^6	10^6
8	512	100000	250000	500000	10^8
10	512	200000	350000	10^6	10^7

Table 1: Parameters of the simulated tempering runs.

L	Samples	N_{TERM}	N_{MEASURES}
8	4096	400000	2×10^6
10	2048	500000	10^6
12	2048	10^6	10^6
16	900	10^6	10^6

Table 2: Parameters of the parallel tempering runs.

N_{MEASURES} sweeps, like the ones we just described, during which we measure and average the physical quantities. We show the parameters of the parallel tempering in table (2). For the $L \leq 12$ lattice we have used temperatures ranging from 1.3 to 0.7 with a step of 0.05, while that for the $L = 16$ lattice we have taken T ranging from 1.8 down to 0.7 with a step of 0.05.

As we said checking thermalization has been one of the crucial issues of this work. We have checked the following facts:

1. In the both updating schemes the time that a system spends with a given temperature must be independent of the temperature. By construction this fact holds only at equilibrium. All our runs verify this property.
2. The acceptance factor for the temperature update has been monitored, and kept in the range $0.2 - 0.5$.
3. A set of relations among expectation value has been recently proven by Guerra [21] (see also [22, 23]). These relations are satisfied at equilibrium. All our measurements satisfy them with a small error.
4. The single sample probability distributions of the order parameter $P_J(q)$ have to be symmetric for $q \rightarrow -q$. We have verified this symmetry.
5. We have monitored the growth of the spin glass susceptibility and the overlap Binder cumulant. The times that these quantities need to reach their plateau values are estimates of thermalization times. We have kept them under control.

4 The Binder Cumulant and the Susceptibility

We will start by discussing our analysis of the overlap Binder cumulant, supporting the existence of a spin glass phase transition [1, 2]. We show our data in figure (1). A magnified

view is in figure (2): it makes clear the crossing (the signature of a phase transition) between the $L = 4$ and $L = 16$ curves and the $L = 8$ and $L = 16$ curves. From figure (2) a first (qualitative) guess for the critical temperature is

$$T_c \simeq 0.98 \pm 0.05 . \quad (15)$$

These results support and improve the results of [1], where the crossing was first observed. Here we offer evidence for a split of the curves in the low T -region down to $T \simeq 0.7T_c$ (improving over the single point at $T \simeq 0.9T_c$ of [1]). We notice that the splitting is much smaller in the spin glasses than in usual ferromagnets because also in the infinite volume limit, if replica symmetry is broken, the Binder cumulant is not identically equal to one in the low temperature phase, but it is given by

$$g = \frac{3}{2} - \frac{1}{2} \frac{\int dq P(q) q^4}{(\int dq P(q) q^2)^2} . \quad (16)$$

The small dependence of g on L reflects the mild dependence of $P(q)$ on the size. It is evident that g does not go to 1 at $T < T_c$ (see fig. (3)) implying that the function $P(q)$ does not tend to a delta function in the infinite volume limit

The second information that we can obtain from the analysis of the Binder cumulant is the value of the ν critical exponent. We have estimated the value of the exponent ν by fitting the derivative of g in the high temperature region with the technique introduced in [24]. We introduce the function f as the derivative of the Binder cumulant g with respect to T at fixed value of $g = g_0$:

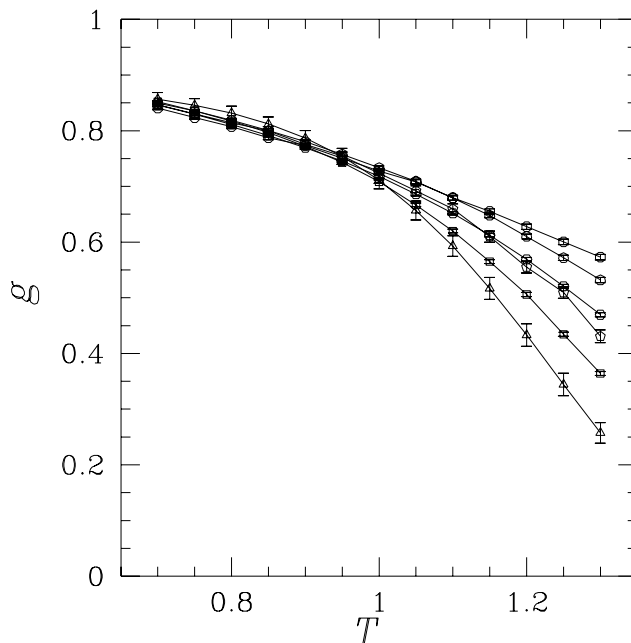


Figure 1: The overlap Binder cumulant versus T for $L = 4, 6, 8, 10, 12$ and 16 (curves from top to bottom on the right part of the figure).

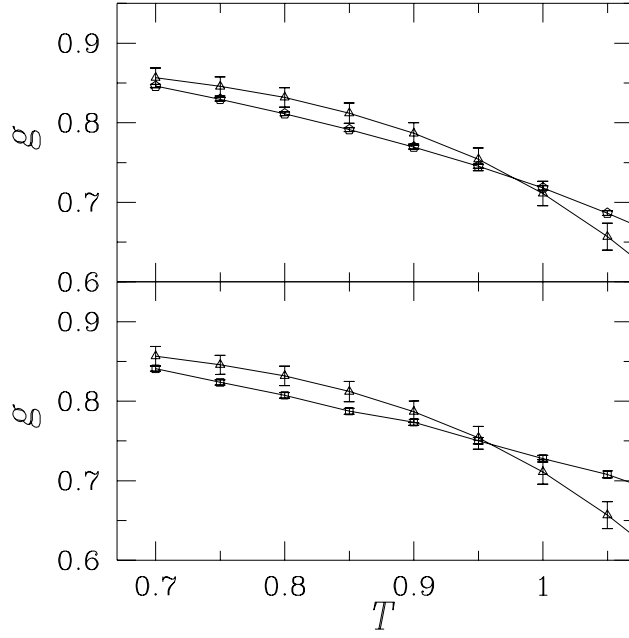


Figure 2: A magnified view of figure (1). In the upper window crossing between the $L = 8$ and $L = 16$ lattices. In the lower window crossing between $L = 4$ and the $L = 16$ lattices.

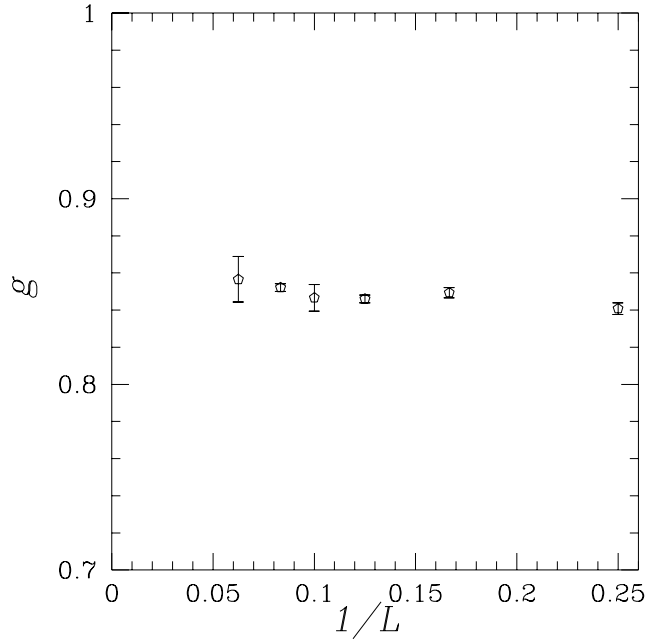


Figure 3: The overlap Binder cumulant at fixed $T = 0.7$ versus $1/L$.

$$f(g_0, L) \equiv \left. \frac{dg}{dT} \right|_{T_0: g(T_0)=g_0} \simeq \alpha L^{\frac{1}{\nu}} . \quad (17)$$

We have computed the derivatives of the overlap Binder cumulant in the range from $g = 0.6$ to $g = 0.8$ (the crossing point is close to the value 0.75). In this interval we have fitted the Binder cumulant curves (at fixed L) using fourth and fifth order polynomials (in order to control the systematic effects due to the fitting procedure). To cross check consistency we have also used a derivative both with respect to the temperature and with respect to β : the two procedures are equivalent and they should produce the same result.

In a large region with $T > T_c$ close to the critical point such an estimate turns out to be, as hoped and expected, independent of the g_0 value that has been used. We plot in figure (4) the values of $\frac{1}{\nu}(g_0)$ as a function of g_0 (obtained fitting the data with a fourth degree polynomial both in T and in β). We expect the fit to collapse when going too close to g_c because of the large error involved.

The fit to the power behavior of eq. (17) works well in the range of g_0 going from $g_0 = 0.6$ to $g_0 = 0.68$ (i.e the $\chi^2/\text{DF} \simeq 1$, DF stands for degrees of freedom): for $g_0 \geq 0.69$ we get too close to the crossing and the fit becomes unfaithful. This happens both for the β and the T fit. The error looks bigger in the β interpolation. The final value is

$$\nu = 2.00 \pm 0.15 . \quad (18)$$

Let us stress the “locality” of this method. We perform the derivative closer and closer the critical point. When we determine a plateau we know we are entering the critical region where scaling violations are small.

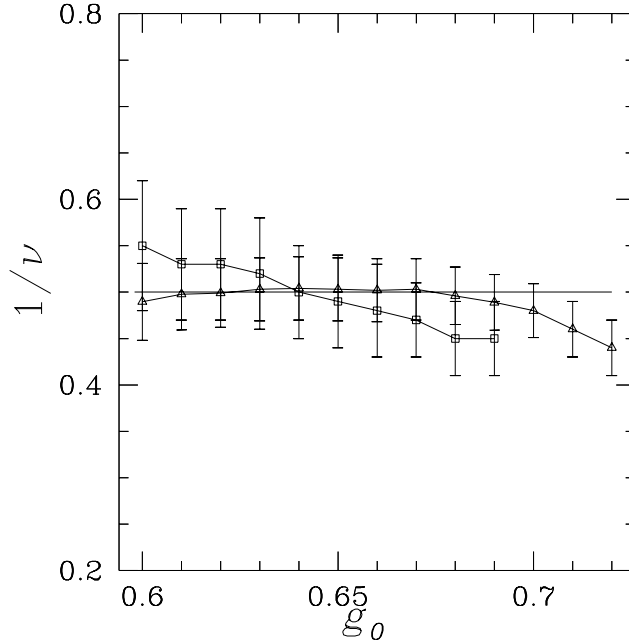


Figure 4: $\frac{1}{\nu}(g_0)$ versus g_0 . Triangles for fits over T , squares for fits over β .

g_1	T_c	$1/\nu$
0.60	1.03 ± 0.02	1.5 ± 0.5
0.65	1.03 ± 0.02	1.5 ± 0.5
0.66	1.03 ± 0.02	1.7 ± 0.5
0.67	1.02 ± 0.02	1.9 ± 0.6
0.68	1.01 ± 0.01	2.2 ± 0.6
0.69	1.01 ± 0.01	2.5 ± 0.7
0.70	1.00 ± 0.01	3.0 ± 0.8

Table 3: Values of the critical temperature and the ν -exponent extracted from the g_1 analysis of the overlap Binder cumulant.

The Binder cumulant also gives us quantitative information about the value of the critical temperature. One can see [15] that the temperature where the Binder cumulant takes a given value, that we call $g_1 \equiv g(L, T_c(L, g_1))$, close enough to g_c , scales as

$$T_c(L, g_1) = T_c(\infty) + aL^{-1/\nu} . \quad (19)$$

Such a value of the infinite volume critical temperature and of the critical exponent will depend on g_1 if it is not close enough to g_1 : when taking the infinite volume limit we have to keep g_1 close enough to g_c . Inside the critical region we will find that asymptotically the critical temperature and the critical exponent become independent of g_1 . We give in table (3) our results. All the fits of the table have a good χ^2/DF . In this analysis we have used only the data from lattices with $L \geq 6$. From table (3) we obtain

$$T_c = 1.02 \pm 0.02 , \quad \nu = 1.9 \pm 0.6 . \quad (20)$$

This determination of ν has a very large error. We can use the more accurate estimate of (20) to obtain the best final estimate of T_c . For example if we fix $\nu = 2$ in (19) we find $T_c = 1.040 \pm .003$ for $g_1 = 0.65$; $T_c = 1.015 \pm 0.004$ for $g_1 = 0.68$ and $T_c = 0.992 \pm 0.003$ for $g_1 = 0.70$. For $g_1 > 0.70$ the quality of the fit is poor. Taking into account all these numerical results and the ν 's error bars [29] we finally quote the result

$$T_c = 0.99 \pm 0.03 , \quad \nu = 2.00 \pm 0.15 . \quad (21)$$

We end this quantitative study with the standard plot of the overlap Binder cumulant, in figure (5): we plot g versus the scaling variable $L^{1/\nu}(T - T_c)$, using $\nu = 2.0$ and $T_c = 0.99$.

After locating with good precision the location of the critical point we can study the divergence of the spin glass susceptibility. The susceptibility diverges with a power law with an exponent given by $\frac{\gamma}{\nu}$. Fitting our data at $T_c = 0.99$ we obtain $\frac{\gamma}{\nu} = 2.30$. We must take into account the error bars on the critical temperature. At $T = 0.99 + 0.03$ we find $\frac{\gamma}{\nu} = 2.24$ while at $T = 0.99 - 0.03$ we have $\frac{\gamma}{\nu} = 2.36$, so we quote

$$\frac{\gamma}{\nu} = 2.30 \pm 0.06 . \quad (22)$$

These exponents are in good agreement with those found by Kawashima and Young [1] for the $J = \pm 1$ Ising spin glass, $\nu = 1.7 \pm 0.3$ and $\frac{\gamma}{\nu} = 2.35 \pm 0.05$, and with the $\frac{\gamma}{\nu} = 2.37 \pm 0.04$ found by Berg and Janke in [2].

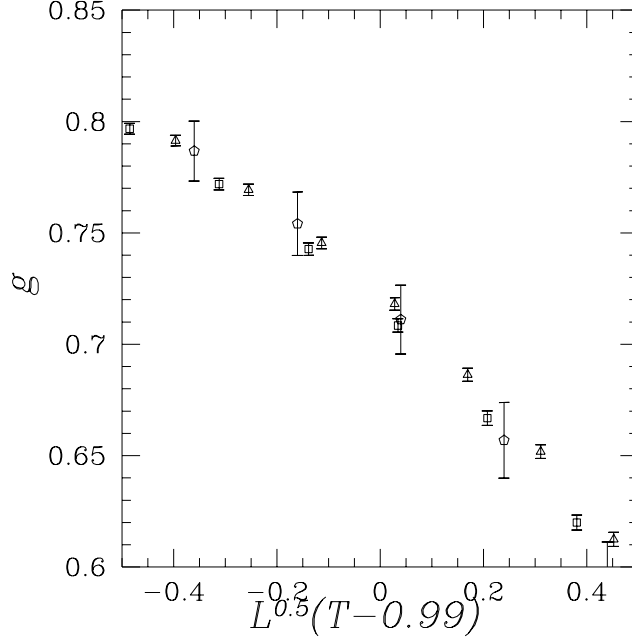


Figure 5: g versus $L^{\frac{1}{2}}(T - T_c)$, with $\nu = 2.0$ and $T_c = 0.99$. In the precision given by the statistical error all the points (from different lattice sizes) collapse on the same curve. Triangles for $L = 8$, squares for $L = 12$ and pentagons for $L = 16$.

5 Analyzing $P(q)$

In this section we analyze the overlap probability distribution $P(q)$. The $P(q)$ is a crucial ingredient of the RSB picture: its equilibrium non trivial shape implies a whole series of unusual patterns of behaviors. The average properties of the function $P(q)$ have been discussed in reference [25]. The results are shown at the lowest temperature in figure (6). The position of the peak (q_M) was fitted as (at the lowest temperature we considered, $T = 0.7$)

$$q_M = (0.70 \pm 0.02) + (1.6 \pm 0.7)L^{-(1.5 \pm 0.4)} . \quad (23)$$

Let us discuss how the system develops with increasing L a Dirac delta function at $q = q_{EA} \simeq 0.7$. We define

$$A(L) \equiv \int_{q_{\max}}^1 d|q| P_L(|q|) , \quad (24)$$

where $q_{\max}(L)$ is the overlap value where $P_L(|q|)$ is maximum. If in the infinite volume limit the system develops a Dirac delta function at $q_{EA} = 0.7$ $A(L)$ should not depend on L (at least for L large enough). The weight of the Dirac delta will be $2A$ (if the delta is approximated by a symmetric function).

For instance at $T = 0.7$ we find $A(4) = 0.25 \pm 0.03$, $A(6) = 0.27 \pm 0.01$, $A(8) = 0.26 \pm 0.01$, $A(10) = 0.22 \pm 0.05$, $A(12) = 0.27 \pm 0.03$ and finally $A(16) = 0.25 \pm 0.04$. We

can assume that the previous values are roughly constant ($A \simeq 0.26 \pm 0.02$), and we expect that the weight of the Dirac delta at $q_{EA} = 0.7$ will be, if the delta is approximated by a symmetric function, 0.52 ± 0.04 . This implies that it is consistent to assume that the peak will become a delta function in the infinite volume limit. In any case the weight must be substantially larger than 0.26.

Moreover this result supports the existence of a continuous part of $P(q)$ between 0 and $q_{EA} = 0.7$, that carries the missing weight 0.48 (if the delta is approximated by a (almost) symmetric function), in order to make $\int_0^1 dq |P(q)| = 1$. This analysis gives further support to the existence of a replica symmetry breaking phase transition in the 3D EA spin glass.

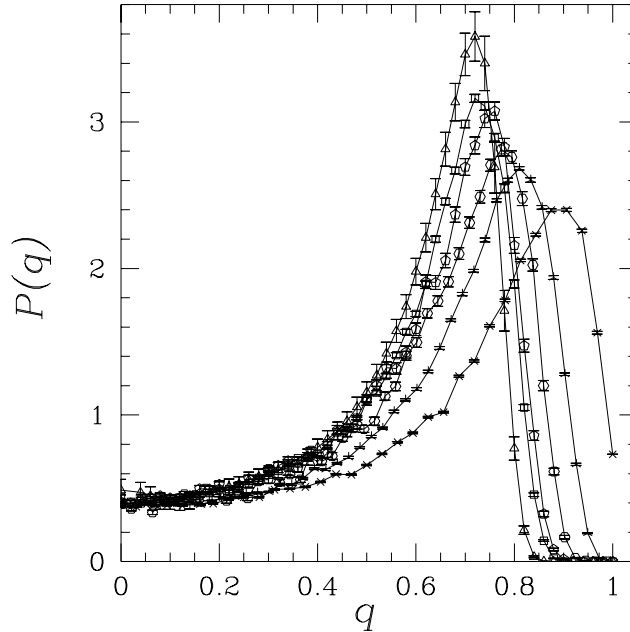


Figure 6: $P(q)$ probability distributions at $T = 0.7$ for all the simulated lattice sizes.

According to the replica predictions the function $P_J(q)$ changes dramatically from sample to sample. A smooth dependence on q is obtained only after average. We show in figure (7) three different functions $P_J(q)$ for three different samples. One can see that different samples have a very different behavior. In the first distribution on the top we have a sizable contribution for $q \simeq 0$: these kind of samples contribute to the low q part of $P(q)$ (exactly like it happens in mean field: only some samples carry weight at $q \simeq 0$, while some samples have a zero probability for $q \simeq 0$ overlaps). The sample in the middle has five clear maxima, one in $q = 0$ and four at high q values. The lower sample has 4 very sharp minima (here the similarity with a δ function starts to be clear), and close to no weight at $q \simeq 0$. Notice that the level of symmetry of these plots for $q \leftrightarrow -q$ is a good check of how good the thermalization has been.

Here we will compare in quantitative way the detailed predictions of the sample to sample fluctuations of the function $P_J(q)$ with the very detailed predictions of replica theory [26, 27], and we will find a remarkable agreement.

From the $P_J(q)$ of (4) we define the integrated probability distribution

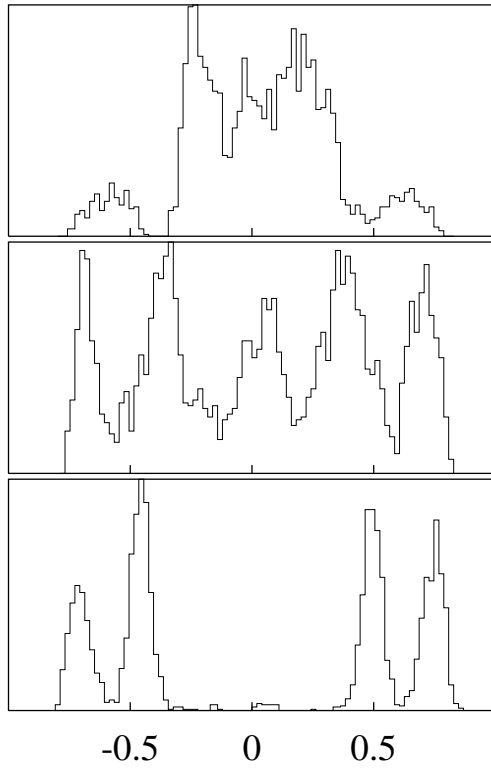


Figure 7: Non normalized $P_J(q)$ (histogram) for three different realizations of the quenched disorder, $L = 16$ and $T = 0.7$.

$$x_J(q_s) \equiv \int_0^{q_s} dq P_J(q) \equiv 1 - y_J(q_s) , \quad (25)$$

i.e. the total probability that the overlap in a given sample is smaller than q_s . In the following q_s will be kept fixed. The probability distribution of $x_J(q_s)$, that following [27] we denote by $\hat{\Pi}_{q_s}(x_J)$, is also a random variable, and it depends on the disorder realization J . In order to get a better statistical signal (for reasons that will become clearer in the following) it is useful to define the integrated probability of $\hat{\Pi}_{q_s}(x_J)$

$$\hat{\Pi}_{q_s}^<(r) = \int_0^r dz \hat{\Pi}_{q_s}(z) . \quad (26)$$

We define also

$$x(q_s) \equiv \overline{x_J(q_s)} = \int_0^{q_s} dq P(q) \equiv 1 - y(q_s) . \quad (27)$$

With our numerical simulations we compute $P_J(q)$ for every realization of the quenched disorder J . We select a fixed value of q_s , and for each realization J we compute the probability to find at equilibrium an overlap smaller than q_s . The answer to the question “for which percentage of disorder realizations such a probability is smaller than r ?” is given by $\hat{\Pi}_{q_s}^<(r)$. This procedure is repeated for a set of q_s values (in the numerical work we have used $q_s = 0.1, 0.2, \dots, 0.9$, see below).

The properties of this distribution have been carefully studied in the past [26, 27] in the framework of the Mean Field RSB theory. An analytic expression can be obtained for it; indeed one can prove that [27]

$$\int_0^\infty dv e^{-zv} g_{q_s}(v) = \frac{1 - x(q_s)}{z} \frac{D_{x(q_s)-2}\left(\frac{-1}{\sqrt{2z}}\right)}{D_{x(q_s)}\left(\frac{-1}{\sqrt{2z}}\right)}, \quad (28)$$

where $\Pi_{q_s}(y_J) \equiv \hat{\Pi}_{q_s}(1 - x_J)$ (i.e. it is the probability distribution of the random variable $y_J(q_s)$), and

$$g_{q_s}(u) \equiv \int_0^1 dz \Pi_{q_s}(z) e^{\sqrt{u/z}}. \quad (29)$$

The D_α are the parabolic cylindric functions, and $x(q_s)$ has been defined in (27).

The function $\Pi_{q_s}(z)$ has many interesting properties. We will concentrate on some of the asymptotic properties of $\Pi_{q_s}(z)$ for z close to 1. It has been proven that the previous formulae imply that:

$$\Pi_{q_s}(z) \simeq (1 - z)^{x(q_s)-1} \quad \text{as } z \rightarrow 1, \quad (30)$$

or equivalently

$$\hat{\Pi}_{q_s}(z) \simeq z^{x(q_s)-1} \quad \text{as } z \rightarrow 0. \quad (31)$$

Finally, in terms of the integrated probability distribution

$$\hat{\Pi}_{q_s}^<(z) \simeq z^{x(q_s)} \quad \text{as } z \rightarrow 0. \quad (32)$$

The integrated probability distribution from 0 to z (for a fixed reference value q_s) goes to zero (when $z \rightarrow 0$) as a power law of z with exponent $x(q_s)$. What we are looking for is the probability of finding a function $P_J(q)$ which is very small in the region $0 < q < q_s$ (i.e. $\int_0^{q_s} dq P_J(q) < z$), and this probability goes to zero as a power of z . This behavior is quite peculiar, especially in the region where $x(q_s)$ is small. Indeed we find that $\hat{\Pi}_{q_s}^<(z)$ remains a quantity of order 1 as far as we stay in the region

$$z > e^{-\frac{1}{x(q_s)}}. \quad (33)$$

When $x(q_s)$ is small the probability distribution of z becomes very *intermittent*

$$\begin{aligned} \overline{z} &= x(q_s) \\ e^{\overline{\log(z)}} &= e^{-\frac{1}{x(q_s)}}. \end{aligned} \quad (34)$$

Where $\log x$ means, in the whole paper, the natural logarithm of x . Before using our numerical simulations of the 3D model to check if we find a similar power behavior, it is convenient to look more closely to the analytic predictions. In the RSB solution of the mean field theory one can directly inspect the solution (28) to exhibit the power law behavior. However the computation of the function itself is rather lengthy because it involve the evaluations of inverse Laplace transforms. Let us illustrate here a different way to obtain the correct answer, which is based on probabilistic techniques and has also the advantage of giving a further insight in the features of the RSB solution.

We recall that in the RSB theory the ultrametric structure of the states implies that it is possible, by fixing a given value of the overlap q_c , to break the set of all the pure

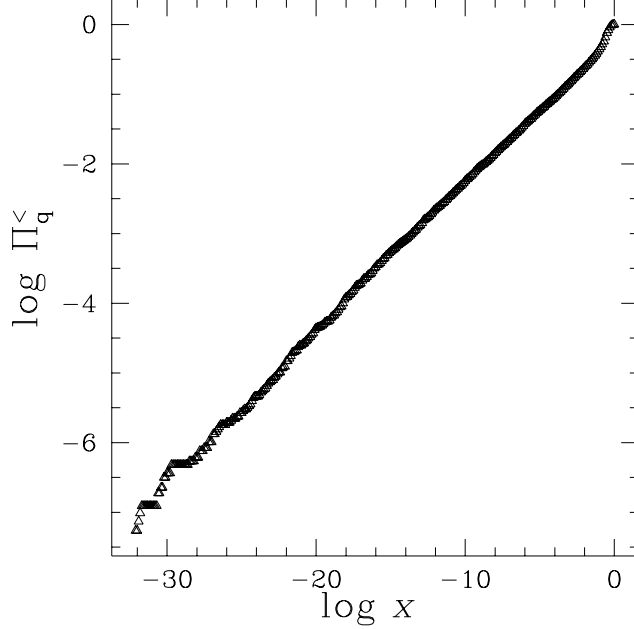


Figure 8: $\log(\Pi_q^<(x))$ versus $\log(x)$ in the mean field approximation. Here q has been fixed to a value such that $x_c = 0.2$ (see text). The clear power law behavior is well fitted by an exponent equal to x_c .

states in clusters [26]. Two pure states belong to the same cluster if their mutual overlap is bigger than q_c . This is equivalent to fix a value of $x_c \equiv x(q_c)$, since the relation between q and x is monotonic (see equation (27)). Each cluster is characterized by a weight w_I^J , where I is the index of the cluster and J means that we are working in a given disorder realization, that is nothing but the sum of the weights of all the pure states belonging to the cluster. The probability of finding an overlap greater than q_c (the reference value in the construction of the clusters) turns out to be

$$y_J(q_c) \equiv 1 - x_J(q_c) = \sum_I (w_I^J)^2, \quad (35)$$

where the index I is running over all the clusters [30].

A theoretical analysis tells us that the probability distribution of the weights of the clusters can be generated by the following algorithm. We consider a system where N clusters are allowed (eventually N will go to infinity). We assign the weights w_I to the N clusters as follows

$$w_I = A e^{-\beta F_I}, \quad (36)$$

where F_I is the extensive free energy of cluster I , and A is a (F -dependent) normalization constant such that $\sum_{I=1,N} w_I = 1$. The extensive free energies are mutually independent and they are distributed according to

$$P(F_I) = \begin{cases} B e^{\beta x(q_c) F_I} & \text{if } F < F_M, \\ 0 & \text{otherwise} \end{cases} \quad (37)$$

where B is a normalization factor. With these weights we can construct the quantity $1 - \sum_I w_I^2$ and compute the probability distribution of these sums (the $\hat{\Pi}_{q_c}$) or the integrated probability distribution $\hat{\Pi}_{q_c}^<(r)$. The result for the weights does not depend on F_M , which we can take equal to 0. If we use this algorithm in the limit where $N \rightarrow \infty$ we obtain the correct probability distribution.

This algorithm can be easily implemented numerically. The probability distribution of the quantity $\omega_I \equiv \exp(-\beta F_I)$ is given by

$$P_{q_c}(\omega) \propto \frac{1}{\omega^{x(q_c)+1}} \quad (38)$$

can be now generated by extracting N weights w using the random numbers p , uniformly distributed in $(0, 1)$: $w = A \frac{1}{p^{1/x_c}}$. With these weights we can construct the quantity $1 - \sum_I w_I^2$ and compute the probability distribution of these sums (the $\hat{\Pi}_{q_c}$) or the integrated probability distribution $\hat{\Pi}_{q_c}^<(r)$.

Very good results can be obtained also for moderate values of N (i.e. $N > 10$ if we do not consider a value of x close to 1. We show in figure (8) the result of this algorithm for a choice of q_c such that $x_c = 0.20$. As it should be the data follow a very accurate power law in the range of $\log(x)$ going to -25 to -1 , with an exponent of 0.2.

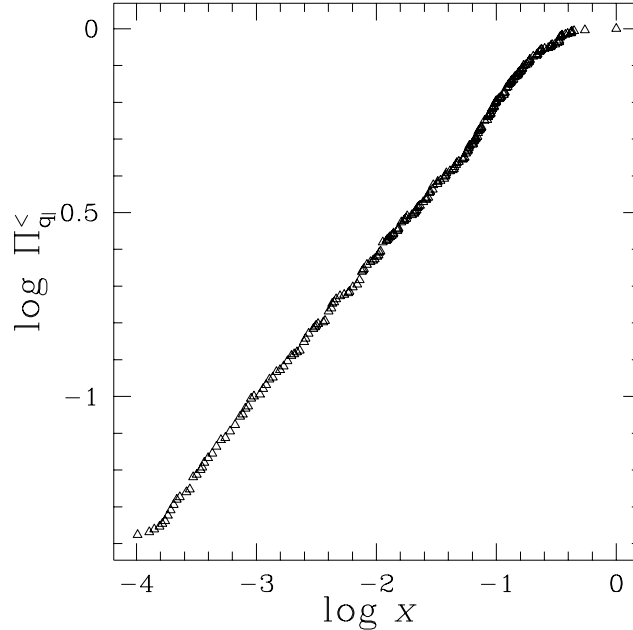


Figure 9: $\log \Pi_q^<(x)$ versus $\log x$ from the results of numerical simulations of the 3D Edwards Anderson spin glass. Here $q = 0.3$ (which corresponds to $x_c = x(0.3) \simeq 0.15$), $L = 16$ and $T = 0.8$.

We plot the results for $\hat{\Pi}_{q_c}^{\leq}(r)$ from the numerical simulations of the 3D model in figure (9). The power law behavior is clear, and consistent with the results of mean field theory. The exponent $x_{3D}(q_c)$ does not coincide exactly, as a function of q_c , with the function $x(q_c)$ (calculated by integrating directly the equilibrium $P(q)$): we plot the two functions in figure (10).

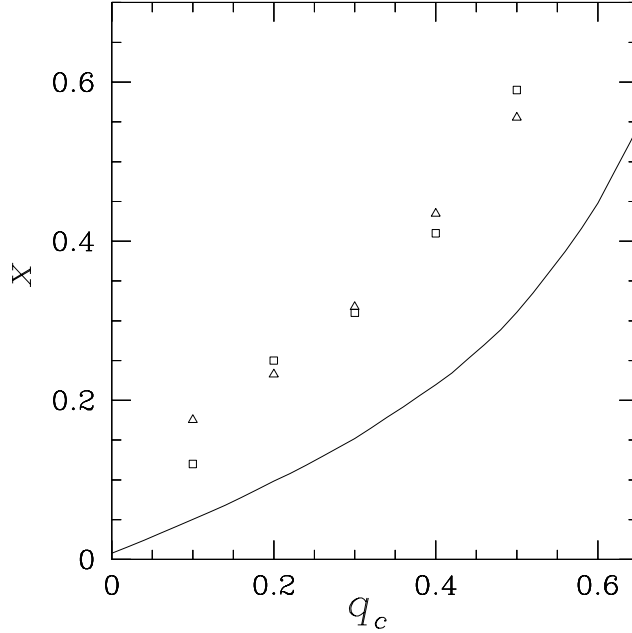


Figure 10: The exponent $x_{3D}(q_c)$ obtained on a $L = 10$ lattice (squares) and on a $L = 16$ lattice (triangles) at $T = 0.8$. The continuous line is the equilibrium function $x(q)$, obtained by integrating the equilibrium probability function, $P(q)$, using equilibrium data on a $L = 12$ lattice.

We can obtain more insight about $P(q)$ by analyzing the moments of the $\hat{\Pi}_{q_c}(r)$ probability distribution. We consider the relations [26], valid in the RSB solution of the mean field model,

$$x_2(q_c) = \frac{1}{3}x_1(q_c) + \frac{2}{3}x_1^2(q_c) , \quad (39)$$

$$x_3(q_c) = \frac{x_1(q_c)}{15} \left(3 + 7x_1(q_c) + 5x_1(q_c)^2 \right) , \quad (40)$$

where

$$x_n(q_c) \equiv \int dr \, r^n \hat{\Pi}_{q_c}(r) . \quad (41)$$

We plot in figure (11) $\frac{x_2}{x_1}$ versus x_1 for the $L = 8, 10$ and the $L = 16$ lattices at two different temperatures: $T = 0.8$ and $T = 0.7$. We also show the straight line prediction of mean field theory (39). We note the numerical data do not depend on the temperature. The

figure also shows that for $x > 0.5$ there is a good agreement among the mean field RSB solution and the numerical data for the 3D model. For $x < 0.5$ data on larger lattices are becoming closer to the mean field result. Recent analytic and rigorous work [21, 22, 23] is focusing on relations of the type (39), and on the relations among expectation values with different number of replicas.

We have obtained similar results analyzing x_3/x_1 against x_1 . Our numerical data are plotted in figure (12) together with the Mean Field prediction of equation (40)).

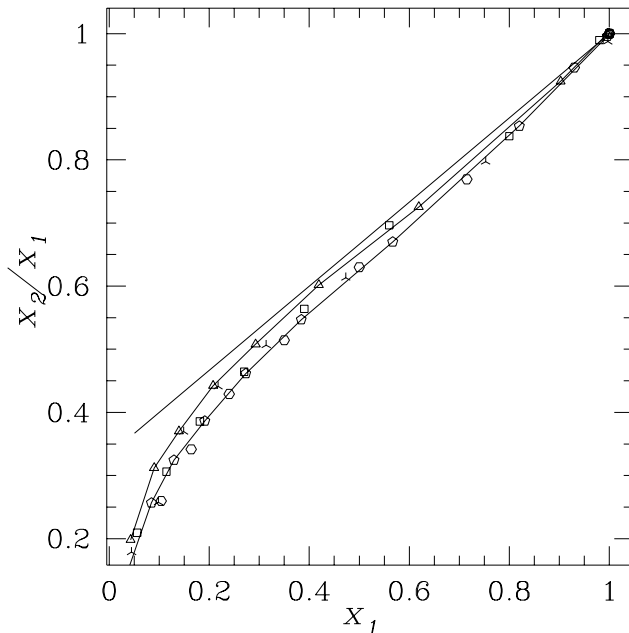


Figure 11: $\frac{x_2}{x_1}$ versus x_1 . For $L = 10$ $T = 0.7$ (triangles), and $T = 0.8$ (squares); for $L = 8$ $T = 0.7$ (pentagons), and $T = 0.8$ (hexagons); for $L = 16$ at $T = 0.7$ (heptagons) Triangles and pentagons are connected with continuous lines. The straight line is the mean field prediction.

We have seen that the replica predictions are in good agreement with the numerical data. There are however two problems:

- the relations (39) and (40) seems not to work at small x_1 ;
- the value of the dynamical exponent $x_{3D}(q_c)$ is higher than what it should be.

It is not clear from our data if these discrepancies are a finite volume effects or if they disappear when the volume goes to infinity. We want to point out that these discrepancies are just what we would expect from finite size effects. Indeed in a finite volume we could expect that

$$P(q) = \sum_{\alpha, \beta} w_{\alpha} w_{\beta} f(q - q_{\alpha, \beta}, \Delta_{\alpha, \beta}) , \quad (42)$$

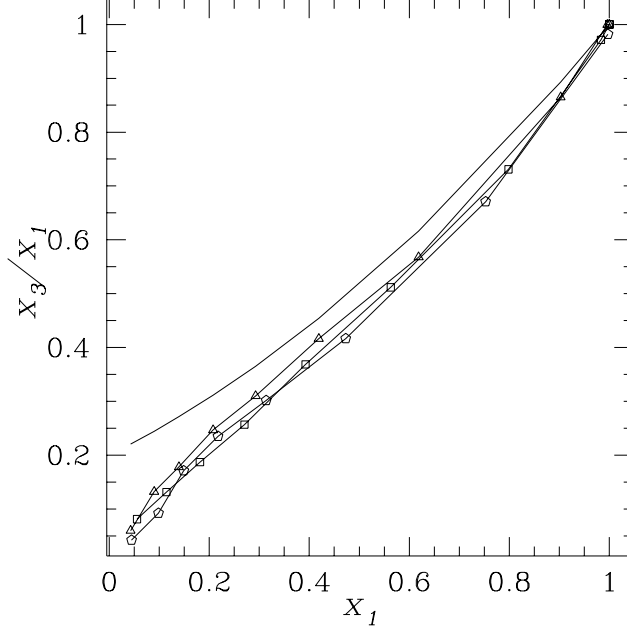


Figure 12: $\frac{x_3}{x_1}$ versus x_1 . For $L = 10$ $T = 0.7$ (triangles), and $T = 0.8$ (squares). For $L = 10$ $T = 0.7$ (pentagons). The upper continuous line is the mean field prediction.

where the function $f(z, \Delta)$ is essentially different from zero for $|z| < \Delta$. In the limit $\Delta \rightarrow 0$ we should have $F(z, \Delta) \rightarrow \delta(z)$. It is obvious that delta function only appears in the infinite volume limit and the quantity Δ is likely to go to zero in the average as a power of L . In this situation the quantity x_J is always of order q when q goes to zero (the function $P_J(q)$ being bounded) and therefore the expectation of x_J^2 is of order q^2 . Consequently in the region where $q < \Delta$ we must have that the ratio $\frac{x_2}{x_1}$ must go to zero with x . It is remarkable that this behavior sets in only at small values of x_1 .

The same argument can be applied to the tails of the probability distribution. For sake of simplicity we consider the case where

$$f(z, \Delta) = \frac{\theta(\Delta^2 - z^2)}{2\Delta}. \quad (43)$$

It is evident that the value of $P(q)$ will be affected by the presence of states having an average overlap different at most Δ from q . A simple computation show that in the approximation where Δ does not depend on the states α and β , we have that

$$x_{3D}(q_c) = x(q - \Delta), \quad (44)$$

which is roughly what we observe, with $\Delta \approx 0.15$. This value is of the same order of magnitude of the width of the function $P(q)$ at the peak and also is of the same order of magnitude of the region, in x_1 , in which the relations (39) and (40) do not work. A much more accurate analysis is needed to decide if these small discrepancies arise from the mechanism outlined here and consequently disappear at large volumes.

6 A Simple Function

Let us consider the function

$$\beta(1 - \overline{\langle |q| \rangle}) , \quad (45)$$

that we will call F . In the RSB solution of the mean field model one can compute its behavior. Usual arguments imply that $F = \chi$, χ being the magnetic susceptibility. In the high temperature phase $P(q)$ is a delta function, and $\overline{\langle |q| \rangle} = 0$: everybody agrees that this result also holds in finite dimensional, realistic spin glasses.

In the SK model one finds that

$$\overline{\langle |q| \rangle} = 1 - T/T_c \quad (46)$$

so that F is exactly constant.

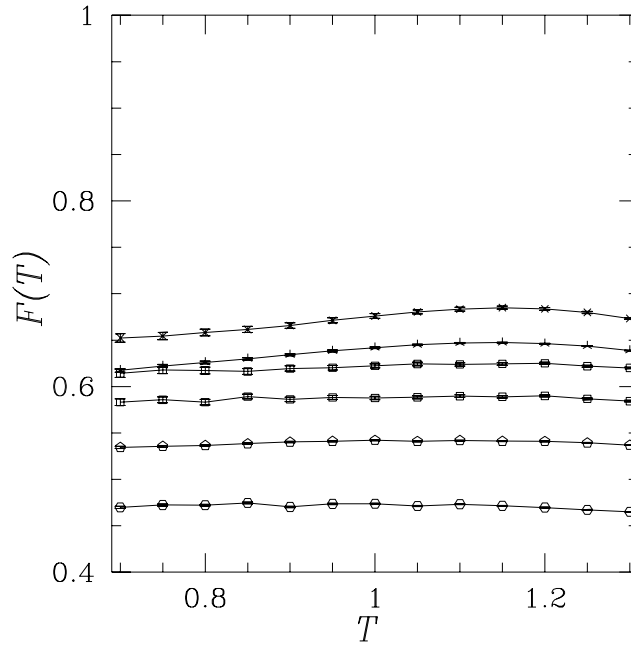


Figure 13: $F(T)$ versus T for $L = 4 \dots 16$.

This behavior will be in any cases changed by renormalization at finite D ; $\overline{\langle |q| \rangle}$ does not go to zero but it is proportional to $(1 - T/T_c)^\beta$, where the exponent β is equal to $\frac{1}{2}\nu(1 - \eta)$, which in three dimensions is not far from 1 (our best estimate is $\beta = 1.30 \pm 0.12$).

It is interesting to study how much in 3D this function stays close to a constant in the cold phase also because it should equal to the magnetic susceptibility. We plot F in figure (13) for different values of L : the function turns out to be remarkably constant for $T < T_c$, where q has a highly non-trivial behavior.

7 The Correlation Functions

In reference [6] the $q = 0$ ergodic component of the overlap correlation function was computed by using an off-equilibrium dynamics. The off-equilibrium approach was used since it is difficult to thermalize large lattices in the cold phase, and an extrapolation procedure was used to deduce the equilibrium decay rate on the relevant distance scales. The power law decay of this correlation function gives strong support to the validity of the mean field picture in finite dimensional systems. Here we are able to compute the same correlation functions directly at equilibrium, and to show that we find a completely consistent result, giving in this way even larger support to the validity of the RSB Ansatz for describing realistic spin glasses.

We recall the definition of the equilibrium non-connected correlation function. For each pairs of configuration σ and τ we define the correlation $C(x)$ as

$$C(x) = \frac{1}{L^3} \sum_y \sigma(x+y)\sigma(y)\tau(x+y)\tau(y) . \quad (47)$$

It may be convenient to recall that $C(x)$ does not change under a global flip of the σ or τ configurations. If we restrict the statistic over configurations that have a given overlap q , the correlation function that we will obtain will be denoted by $C_q(x)$ or $C(x|q)$.

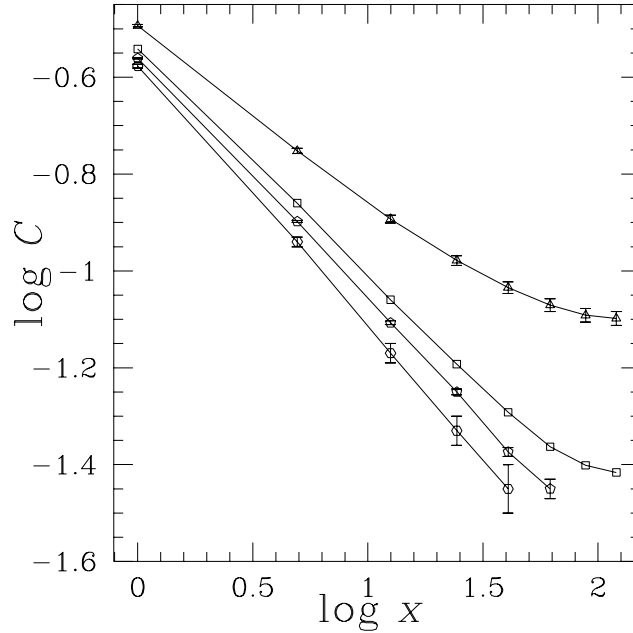


Figure 14: The lower curve is the infinite time extrapolation of the non-equilibrium correlation function $C_d(x|q=0)$ obtained by a sudden quench ($L = 64$). The second curve from the bottom is $C_d(x|q=0)$ obtained by a slow annealing ($L = 64$). The third curve is the equilibrium correlation function computed with the constraint $|q| < 0.01$ ($L = 16$). The upper curve is the full equilibrium correlation function, including all configurations ($L = 16$).

The upper curve in figure (14) is the equilibrium correlation function at $T = 0.7$ on the $L = 16$ lattice. The two lower curves are off-equilibrium $q = 0$ correlation functions from [6]: in the lower curve the system was suddenly quenched from $T = \infty$ to $T = 0.7$, while in the second one a slow annealing procedure was used to bring T down to 0.7. In both cases the lattice size was 64. The third curve from the bottom has been computed, by the same configurations used in the upper curve (equilibrium runs at $T = 0.7$ and $L = 16$), including only couples of configurations where $q < 0.01$. This is the real equilibrium $q \simeq 0$ correlation function, where no extrapolations were needed. The agreement with the result of the off-equilibrium runs is very good: only at $x \simeq 8$, close to the center of the periodic lattice, we see an expected discrepancy (the lattice of the off-equilibrium runs had a linear size of 64, and only close to $L = 32$ boundary conditions became relevant). All the three curves are well compatible with a power law decay of the form $x^{-\lambda}$ with $\lambda \approx 0.5$ in agreement with the predictions of [12].

As we have seen the propagator at fixed q is equal to q^2 plus a term which goes to zero at infinity (see eq. (10)). Therefore at large distances x

$$P_C(C(x)) = \frac{P(C(x)^2)}{(2C(x))^{\frac{1}{2}}}, \quad (48)$$

producing a double peak structure, one peak corresponds to the delta function at q_{EA} and the other peak comes from the singular Jacobian (of the transformation $C \propto q^2$) at zero overlap.

If we naively assume that $C_q(x) = a(x) + b(x)q^2$ both peaks are present also for finite x . If we consider a more complicated dependence of $C_q(x)$ at finite x the leftmost peak may disappear and one could be left with a non divergent structure. A divergent peak should however be present for large x .

In order to justify the equality among the dynamical result and the static results at $q = 0$ we can intuitively argue as follows. We define an “effective” potential [31] given by $-\log P(C(x))$. In an off-equilibrium simulation with random initial conditions all the components of the propagator start at zero. Using the effective potential $-\log P(C(x))$ it is clear that the initial $C(x) = 0$ values drifts to the closest minimum, that is given by $C_{\min}(x)$, i.e

$$\lim_{t \rightarrow \infty} C_d(x, t|q = 0) = C_{\min}(x), \quad (49)$$

where $C_d(x, t|q = 0)$ is the dynamic correlation function computed at time t and distance x using a sudden quench from infinite temperature down to $T < T_c$ (so that the initial overlap is zero, fact that we denote with $q = 0$ in the formula).

The equilibrium probability distribution of $C(x)$ should show a double peak structure. The smaller peak should be located at $C_{\min}(x)$, and this value must be equal to the off-equilibrium value $C_d(x, \infty|q = 0)$ in the infinite time limit (i.e. the lower curve of figure (14)). We show these histograms in figures (15) and (16) for $x = 1$ and $x = 3$ respectively. We have also marked with a vertical line the value obtained from the off-equilibrium simulations.

Qualitatively we see that both histograms have a clear peak (for large values of C , that correspond to C_{\max}) and a second maximum or flex point (for lower values of C , that correspond with C_{\min}). We have also shown the value of the infinite time extrapolation of

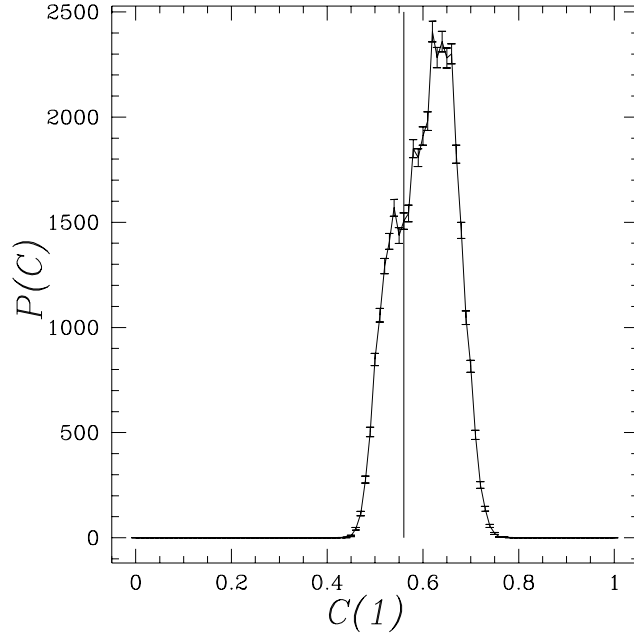


Figure 15: Histogram of the equilibrium correlation function at distance $x = 1$. We have marked with a vertical line the value of $C_d(1, t|q = 0)$ extrapolated to infinite time [6].

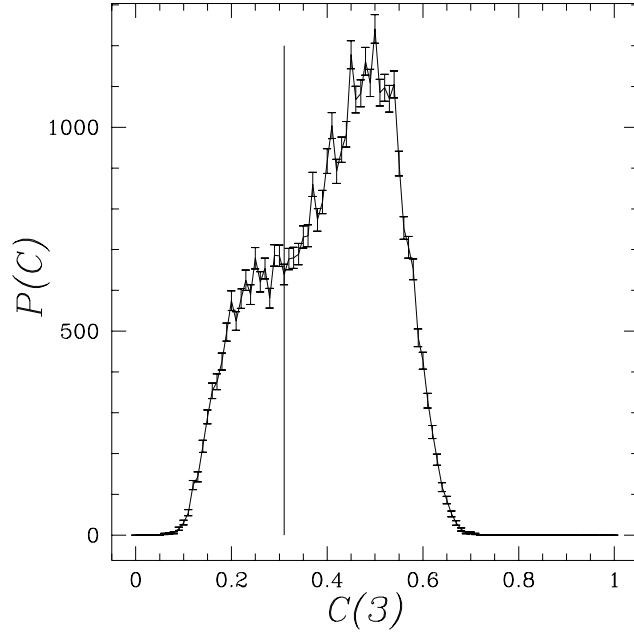


Figure 16: Histogram of the equilibrium correlation function at distance $x = 3$. We have marked with a vertical line the value of $C_d(3, t|q = 0)$ extrapolated to infinite time [6].

$C_d(x, t|q = 0)$ (the vertical line in the plots). The same pattern holds up to $x = 5$ (that is the larger distance that we analyzed in the dynamical runs of [6]). It is clear from figures (15) and (16) that the value of $C(x|q = 0)$ is located close to the second maximum or flex point.

This fact strongly supports the correctness of the off-equilibrium approach for the computation of the $q = 0$ component of the propagator (including the effectiveness of the extrapolation procedure) and confirms that it is possible to compute equilibrium expectation values in off-equilibrium simulations. Moreover the double peak structure of the correlation function probability distribution survives in the infinite volume limit since the dynamical expectation values have been computed on a very large lattice (infinite to all practical effects). It is remarkable that the distribution probability of $C(x)$ becomes wider with increasing x .

All these features of the correlation functions provide a further evidence of the existence of a non trivial probability distribution of the overlaps, and of the fact that finite size effects are well under control.

Finally we can check our previous estimate of the η exponent ($\gamma/\nu = 2 - \eta$, and so $\eta = -0.30(6)$). We recall that at the critical point we have

$$C(x) \propto \frac{1}{x^{D-2+\eta}} . \quad (50)$$

This formula always holds at the critical point.

We show in figure (17) the overlap-overlap correlation function at (almost) the critical point ($T = 1.0$) for $L = 16$. Taking into account the points in the interval $[1, 5]$ we have found a very good power law fit with exponent $1 + \eta = 0.710(5)$, giving $\eta = -0.29$ according with our previous estimate. Obviously for $x > 5$ the propagator is seeing the periodic boundary conditions and the propagator misses the pure power law behavior. We can remark that this early power law behavior that we have found (for $x \geq 1$) have been seen, for instance, in the four and six dimensional Ising spin glass [7, 8].

8 Conclusions

The numerical simulations we have discussed here have allowed to establish some important results, and to make clear some relevant issues. Maybe the main point is that the observed equilibrium behavior of the 3D spin glass shares the crucial features of RSB solution of the mean field theory. We are able to establish that on large lattices, deep in the broken phase.

The study of the overlap Binder cumulant and of the spin glass susceptibility allow a precise determination of the critical exponents. The analysis of sample to sample variations $P(q)$ allows to exhibit clear power law behaviors in the probability distributions that are typical of the mean field theory (and would have no reason to appear in any theory of an usual ferromagnet). Correlation functions are now under control even at equilibrium on large lattices, for the whole set of stable configurations and for the zero overlap part of the phase space.

We believe that a very clear picture is emerging.

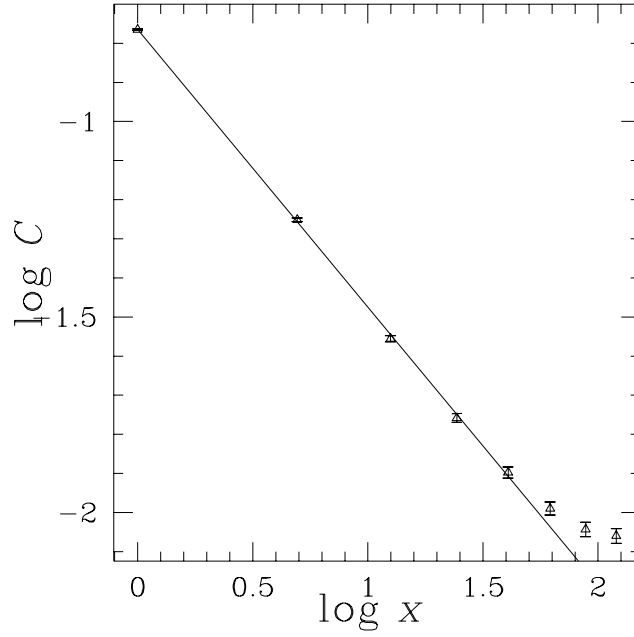


Figure 17: The correlation function at the critical point ($T = 1.0$) for a $L = 16$ lattice in a double logarithmic scale. We have marked with a straight line the results of a power law fit (taking the points in the interval $[1, 5]$). The slope is in very good agreement with the results found by fitting the susceptibility as a function of the lattice size. See the text for more details.

Acknowledgments

J. J. Ruiz-Lorenzo is supported by an EC HMC (ERBFMBICT950429) grant.

References

- [1] N. Kawashima and P. Young, Phys. Rev. B. **53** R484 (1996).
- [2] B. A. Berg and W. Janke, *Multi-Overlap Simulations of the 3d Edwards-Anderson Ising Spin Glass*, cond-mat/9712320 (December 1997).
- [3] C. M. Newman and D. L. Stein, cond-mat/9711010 and references therein; G. Parisi, cond-mat/9603010; E. Marinari, G. Parisi, F. Ricci-Tersenghi and J. J. Ruiz-Lorenzo, to be published; E. Marinari, G. Parisi, F. Ricci-Tersenghi, J. J. Ruiz-Lorenzo and F. Zuliani, to be published;
- [4] E. Marinari, G. Parisi and J. J. Ruiz-Lorenzo, *Numerical Simulations of Spin Glass Systems*, in *Spin Glasses and Random Fields*, edited by P. Young (World Scientific, Singapore 1997), cond-mat/9701016.
- [5] M. Mezard, G. Parisi and M.A. Virasoro, *Spin Glass Theory and Beyond* (World Scientific, Singapore, 1987).
- [6] E. Marinari, G. Parisi, J. J. Ruiz-Lorenzo and F. Ritort, Phys. Rev. Lett **76**, 843 (1996).
- [7] G. Parisi, F. Ricci-Tersenghi and J. J. Ruiz-Lorenzo, J. Phys. A: Math. Gen. **29**, 7943 (1996).
- [8] G. Parisi, P. Ranieri, F. Ricci-Tersenghi and J. J. Ruiz-Lorenzo, *Mean Field Dynamical Exponents in Finite Dimensional Ising Spin Glass*, J. Phys. A: Math. Gen. **30**, 7115 (1997).
- [9] E. Marinari, G. Parisi, F. Ricci-Tersenghi and J. J. Ruiz-Lorenzo, *Violation of the Fluctuation Dissipation Theorem in Finite Dimensional Spin Glasses*, cond-mat/9710120 (October 1997). J. Phys. A: Math. Gen (in press).
- [10] E. Marinari, G. Parisi and F. Zuliani, *4D Spin Glasses in Magnetic Field Have a Mean Field like Phase*, J. Phys. A: Math. Gen. to be published, cond-mat/9703253 (March 1997).
- [11] G. Parisi, F. Ricci-Tersenghi and J. J. Ruiz-Lorenzo, *On the Dynamics of the 4d Spin Glass in a Magnetic Field*, Phys. Rev. B to be published, cond-mat/9711122 (November 1997).
- [12] C. de Dominicis, I. Kondor and T. Temesvari, *Beyond the Sherrington-Kirkpatrick Model*, in *Spin Glasses and Random Fields*, edited by P. Young (World Scientific, Singapore 1997), cond-mat/9705215.
- [13] O. F. de Alcantara, J. E. Kirkham and A. J. McKane, J. Phys. A: Math. Gen. **14**, 2391 (1981).
- [14] G. Parisi, *Statistical Field Theory* (Addison-Wesley, New York).
- [15] G. Parisi and J. J. Ruiz-Lorenzo, Phys. Rev. B **54**, R3698 (1996).

- [16] H. G. Ballesteros et al., Phys. Lett. B **400**, 346 (1997).
- [17] E. Marinari and G. Parisi, Europhys. Lett. **19**, 451 (1992).
- [18] M. C. Tesi, E. Janse van Rensburg, E. Orlandini and S. G. Whillington, J. Stat. Phys.; K. Hukushima and K. Nemoto, J. Phys. Soc. Japan **65**, 1604 (1996).
- [19] E. Marinari, *Optimized Monte Carlo Methods*, lectures given at the 1996 Budapest Summer School on Monte Carlo Methods, ed. by J. Kertesz and I. Kondor, Springer-Verlag, to be published, cond-mat/9612010.
- [20] C. Battista *et al.*, Int. J. High Speed Comp., **5**, 637 (1993).
- [21] F. Guerra, Int. J. Mod. Phys. B **10**, 1675 (1996).
- [22] M. Aizenman and P. Contucci, *On the Stability of the Quenched State in Mean Field Spin Glass Models*, cond-mat/9712129 (December 1997).
- [23] G. Parisi, *On the Probabilistic Interpretation of the Replica Approach to Spin Glasses*, cond-mat/9801081 (January 1998).
- [24] D. Iñiguez, G. Parisi and J. J. Ruiz-Lorenzo, J. Phys. A: Math. Gen. **29**, 4337 (1996).
- [25] D. Iñiguez, E. Marinari, G. Parisi and J. J. Ruiz-Lorenzo, J. Phys. A: Math. Gen. **30**, 7337 (1997).
- [26] M. Mezard, G. Parisi, N. Sourlas, G. Toulouse and M. A. Virasoro, Phys. Rev. Lett. **52**, 1156 (1984); J. Physique **45**, 843 (1984).
- [27] M. Mezard, G. Parisi and M. A. Virasoro, J. Physique Lett. **46**, L-217 (1985).
- [28] G. Parisi, J. Phys. A: Math. Gen. **13**, 1887 (1980).
- [29] For $g_1 = .70$ fixing $\nu = 2.15$ we obtain $T_c = 0.995 \pm 0.003$, while fixing $\nu = 1.85$ we find $T_c = 0.990 \pm 0.004$.
- [30] It is easy to obtain this formula. In terms of the weights of the pure states w_α^J the function $P_J(q)$ is given by

$$P_J(q) = \sum_{\alpha, \beta} w_\alpha^J w_\beta^J \delta(q - q_J^{\alpha, \beta}) , \quad (51)$$

where α and β run over all the pure states. Now,

$$y_J(q_c) = \int_{q_c}^1 dq' P_J(q') = \sum_{\alpha, \beta} w_\alpha^J w_\beta^J \theta(q_J^{\alpha, \beta} - q_c) = \sum_I \sum_{\alpha(I), \beta(I)} w_{\alpha(I)}^J w_{\beta(I)}^J , \quad (52)$$

where the index I runs over the clusters (defined with the reference value q_c) and $\alpha(I)$ and $\beta(I)$ run over all the pure states belonging to the cluster I . Taking into account the fact that $w_I^J = \sum_{\alpha(I)} w_{\alpha(I)}^J$ we finally obtain

$$y_J(q_c) = \sum_I (w_I^J)^2 . \quad (53)$$

[31] The partition function is

$$\mathcal{Z} = \int d[\phi] \exp[-\mathcal{H}[\phi]] . \quad (54)$$

For a given distance x the value of the correlation function at distance x is a function of the field ϕ : $C_x = G(\phi) = V^{-1} \int dy \phi(x+y)\phi(y)$, $V = \int dy$ is the volume of the system. Introducing the factor $1 = \int dC_x \delta[C_x - G(\phi)]$ in (54) we obtain

$$\mathcal{Z} = \int dC_x \int d[\phi] \delta[C_x - G[\phi]] \exp[-\mathcal{H}[\phi]] . \quad (55)$$

We define

$$P[C_x] \equiv \int d[\phi] \delta[C_x - G[\phi]] \exp[-\mathcal{H}[\phi]] \quad (56)$$

the probability of finding a given value of C_x . This allows to define the effective free energy (or effective potential) $F[C_x]$

$$F[C_x] \equiv -\log P[C_x] , \quad (57)$$

such that

$$\mathcal{Z} = \int dC_x \exp[-F[C_x]] . \quad (58)$$

In the thermodynamical limit the partition function will be dominated by the minima of $F[C_x]$, that justifies calling it an “effective potential”.